High-Throughput Ionic Liquid Ion Sources Using Arrays of Microfabricated Electrospray Emitters With Integrated Extractor Grid and Carbon Nanotube Flow Control Structures

Frances Ann Hill, Eric Vincent Heubel, Philip Ponce de Leon, and
Luis Fernando Velásquez-García, *Senior Member, IEEE*

***Abstract*— We report the design, fabrication, and experimental characterization of dense, monolithic, and planar arrays of externally-fed electrospray emitters with an integrated extractor grid and carbon nanotube flow control structures for low-voltage and high-throughput electrospray of the ionic liquid EMI-BF_4 in vacuum. Microfabricated arrays with as many as 1900 emitters in 1 cm^2 were fabricated and tested. Per-emitter currents as high as 5 μA in both polarities were measured, with start-up bias voltages as low as 470 V and extractor grid transmission as high as 80%. Maximum array emission currents of 1.35 mA (1.35 mA/cm^2) were measured using arrays of 1900 emitters in 1 cm^2. A conformal carbon nanotube forest grown on the surface of the emitters acts as a wicking structure that transports liquid to the emitter tips, providing hydraulic impedance to regulate and uniformize the emission across the array. Mass spectrometry of the electrospray beam confirms that emission in both polarities is composed of solvated ions, and etching of the silicon collector electrode is observed. Collector imprints and per-emitter current–voltage characteristics for different emitter array sizes spanning three orders of magnitude show excellent emission uniformity across the array. Performance estimates of the devices as nanosatellite thrusters are provided. [2014-0060]**

***Index Terms*— Electrospray, ionic liquid, multiplexing, MEMS, microfabrication, carbon nanotubes.**

I. Introduction

EFFICIENT high-throughput generation of ions and droplets using electrospray ionization is of great interest for a number of emerging technological applications including high-throughput nanomanufacturing, lab-on-a-chip analytical systems, and nanosatellite electric propulsion. Electrospray ionization is a method to produce a spray of charged droplets and/or ions from a liquid using high electric fields [1]. Conventional electrospray systems supply the ionization liquid to a single emitter through a narrow capillary, resulting in relatively small output currents and mass flow rates; emission throughput is particularly low for the emission of nanosized droplets or ions, which require the supply of exceptionally small flow rates [2], [3]. Multiplexing of emitters has been demonstrated as an effective way to increase the overall throughput of electrospray emission while still maintaining small local flow rates with low beam divergence at each emitter site [2], [4]–[6]. Increased electrospray throughput can lead to substantial improvements in performance for a number of applications. For electric propulsion, the maximum thrust from a single electrospray emitter operating in the mass-efficient ionic regime is in the range of 100 nN; multiplexing can increase thrust levels to the tens-of-micronewtons range necessary for nanosatellite maneuvers [7]–[9]. Electrospray sources are additionally used for etching, thin film deposition and high-resolution imaging [10], [11]; with a single electrospray source, these microfabrication techniques have very low throughput, while parallel electrospray beam sources can enable these functionalities over broad areas [12].

In addition to the benefits of multiplexing, the performance of electrospray systems can be improved by scaling-down the emitters, and microfabrication technologies can be used to batch-microfabricate electrospray emitter arrays [2], [4], [6], [13]–[17]. Advantages of scaling down the emitters using microfabrication techniques include (i) sharper emitter tips that operate at lower voltages, (ii) miniaturized emitters that can be packed into denser arrays to obtain a large number of emission sites per unit area with low beam divergence, and (iii) batch-fabrication of monolithic emitter arrays at low cost.

An electrospray source can generate droplets, ions, or a mixture of droplets and ions, depending on the physical properties of the liquid, the electric field, and the flow rate to the emission site. In the cone-jet mode, droplets are formed from the breakup of the jet ejected from the Taylor cone apex; in this regime, the range of stable volumetric flow rates, Q, depends on the properties of the liquid, according to [18]

$$Q = \frac{\eta^2 \gamma \varepsilon_r \varepsilon_o}{\rho \kappa} \tag{1}$$

Manuscript received February 23, 2014; revised April 7, 2014; accepted April 21, 2014. Date of publication May 16, 2014; date of current version September 29, 2014. This work was supported by the Microsystems Technology Office, Defense Advance Research Projects Agency, under Contract W31P4Q-11-1-0007. Subject Editor A. Luque.

F. A. Hill was with the Microsystems Technology Laboratories, Massachusetts Institute of Technology, Cambridge, MA 02139 USA. She is now with KLA-Tencor, Milpitas, CA 95035 USA (e-mail: fahill@alum.mit.edu).

E. V. Heubel and P. P. de Leon are with the Department of Mechanical Engineering, Massachusetts Institute of Technology, Cambridge, MA 02139 USA (e-mail: evheubel@mit.edu; p_ponce@mit.edu).

L. F. Velásquez-García is with the Microsystems Technology Laboratories, Massachusetts Institute of Technology, Cambridge, MA 02139 USA (e-mail: velasquez@alum.mit.edu).

Color versions of one or more of the figures in this paper are available online at http://ieeexplore.ieee.org.

Digital Object Identifier 10.1109/JMEMS.2014.2320509

where η is a dimensionless parameter that ranges between 1 and 10, γ is the surface tension of the liquid, ε_r is the relative electrical permittivity of the liquid, ε_o is the permittivity of free-space, ρ is the mass density of the liquid, and κ is the electrical conductivity of the liquid. The minimum volumetric flow rate, Q_{min}, at which stable cone-jet emission is observed occurs at $\eta \sim 1$ [18]. For flow rates below Q_{min}, it is possible to emit ions without any droplets if the liquid is sufficiently conductive and has a high surface tension [3], [19], [20].

The flow rate from an electrospray emitter is set by either the flow rate drawn from the Taylor cone or the supply of liquid to the Taylor cone; the emission can therefore be *barrier-limited*, i.e., controlled by the ionization process, or *supply-limited*, i.e., controlled by the supply of liquid to the ionization site. With little or no limit on the supply of liquid to the emission site (e.g., electrospray from a free droplet, the free surface of a liquid pool [18], or a channel that provides little resistance to the flow), the flow rate is barrier-limited and set by the magnitude of the electric field at the surface of the liquid and the properties of the liquid. For an array of low-impedance capillary channels, variations in the local electric field across the array (e.g., due to edge effects, fabrication non-uniformities, or misalignment with the extractor electrode) can result in different flow rates being drawn at each emission site [2]. Moreover, allowing the electric field to set the output flow rate could result in high flow rates that can lead to droplet emission rather than ionic emission [2].

Placing a large hydraulic impedance in series with an emission site has been identified as an effective way to limit the flow rate in order to operate in the ionic regime [5], [21]. The viscous forces caused by the hydraulic impedance restrict the flow of the liquid and can limit the flow rate to a lower value than would otherwise be drawn by the electric field; in this case, the flow is supply-limited. For arrays of emitters, a large hydraulic resistor in series with each emitter site results in uniform array output because the effects of the spatial variations in the electric field are minimized. The objective of an optimized hydraulic impedance in an electrospray ion source is to set flow rates as close to Q_{min} as possible without exceeding that value, in order to maximize the ionic emission current from each emission site without producing droplets. Recently, researchers have reported microfabrication approaches to create a high hydraulic impedance to each emitter of the array by filling-in capillary channels with silica microspheres [5], [22] or by electrochemically etching metallic emitter tips [6], [9], [16]; both approaches have demonstrated emission in the ionic regime. Drawbacks of these approaches include the limited degree to which the hydraulic impedance can be finely tuned, variation of the morphology of the porous material within each emitter and across the array, and the use of internal flow channels that are difficult to clean and can be prone to clogging, which can lead to device failure [9].

Externally-fed electrospray emitters [4], [21], [23] have been proposed as an alternative to the more conventional internally-fed emitters to overcome some of the challenges of working with large emitter arrays for ionic emission, namely high flow rates to the emission sites that lead to droplet emission, non-uniform emission across emitter arrays, and channel clogging. An externally-fed emitter has a solid core that is typically conical in shape, with a wide base and a sharpened tip; liquid is transported from the base of the emitter along a relatively thin layer on the surface of the emitter to its tip, where electric field enhancement is highest and electrospray emission occurs. Since the liquid flows over an open two-dimensional structure, there is a redundancy of flow paths and clogging problems are avoided. Liquid is fed to the emission sites without the need for an external liquid pressure feed system, simplifying the overall electrospray source design. Effective surface-fed electrospray of ions requires spontaneous spreading of the liquid over the surface of the emitters and viscous resistance to the flow in order to limit the flow rate drawn at the tip to values below Q_{min}. These requirements can be met by coating the surface of the emitters with a highly wetting, low-permeability porous medium through which the liquid will flow. As a drawback, externally-fed electrospray emitters have a substantially larger liquid free-surface and therefore, if operated in vacuum, are better fit for ionizing liquids with low vapor pressures; however, this is not an issue for many ionic liquids, including EMI-BF_4, because of their very low vapor pressures.

Our group has previously studied the electrospray of ionic liquids using externally-wetted silicon emitters coated in black silicon [4], [13]. The contact angle of the ionic liquid EMI-BF_4 on silicon with a native oxide is measured to be 38°, so silicon emitters without additional surface coatings are not sufficiently wetting for this application. Black silicon is a roughened silicon surface with nanostructured features that is highly wetting, and successful ion emission has been demonstrated from these emitter arrays with as much as 1 μA of output current per emitter [13]. One of the limitations of black silicon as a wicking structure is the limited degree to which the properties of the black silicon film can be deliberately engineered by tuning the etch process [13], [24].

In this work, a forest of carbon nanotubes (CNTs) is proposed as an alternative to black silicon. CNT forests offer a number of advantages as a surface coating for externally-fed emitters: (i) CNT forests grown using plasma-enhanced chemical vapor deposition (PECVD) are highly wetting due to the combination of high surface energy and nanostructured roughness, (ii) CNTs can be grown conformally, (iii) the porosity of a CNT film, determined primarily by the CNT diameter and packing density, sets the hydraulic impedance of the film and is highly tunable by changing the growth parameters, and (iv) the height of the forest can be grown taller than the maximum height of black silicon to accommodate larger flow rates. The characteristics of a PECVD CNT forest, including the CNT diameter, packing density, height and vertical alignment, can be widely varied and finely tuned by changing the growth conditions [25], [26].

This article is the extended version of a recent report on a batch-microfabricated MEMS multiplexed externally-fed electrospray array with an integrated extractor grid and CNT flow control structures for high-throughput generation of ions from ionic liquids in vacuum [27]. The design has a hierarchical structure that brings together optimized features with associated characteristic lengths that span five orders of mag-

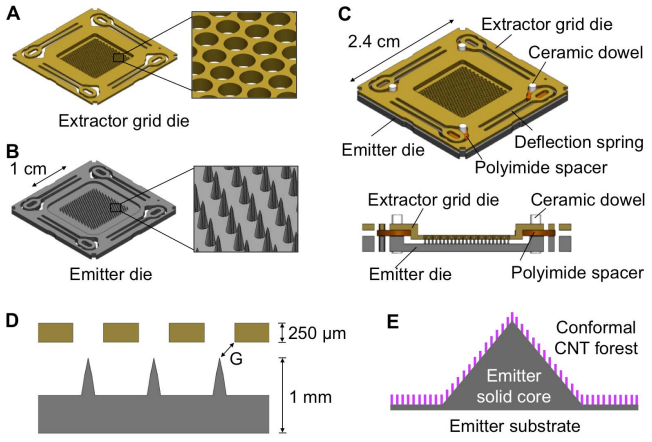

Fig. 1. Schematics of the electrospray source showing (A) the extractor grid die, (B) the emitter die, (C) the assembled device, (D) a close-up of the alignment between the emitter tips and the extractor grid apertures, and (E) a cross-section of an electrospray emitter.

nitude: mesoscale deflection springs [28], [29] for precision assembly of the emitter and extractor electrode dies to attain low beam interception, microsharp emitter tips for low-voltage electrospray emission, and a nanostructured conformal CNT forest that acts as a wicking structure to control the flow rate fed to each emitter and enforce array emission uniformity. To gain insight into the performance of dense arrays of externally-fed emitters with CNT flow control structures, the current-voltage characteristics of electrospray sources with a range of emitter densities are measured, the emission plume is characterized using mass spectrometry, and imprints on a collector electrode are analyzed.

II. Device Structure and Microfabrication

The multiplexed electrospray source is composed of an emitter die and an extractor grid die (Figure 1). Each die is 2.4 cm by 2.4 cm and 1 mm thick. The central 1 cm by 1 cm region of the emitter die is its active area, i.e., it contains the array of emitters. The central 1 cm by 1 cm region in the center of the extractor grid die contains a matching array of circular apertures. Four mesoscale deflection springs etched into each die clamp onto 1/16" outer diameter aluminum oxide dowel pins to align and electrically isolate the two parts. Polyimide spacers fit over the dowel pins to set the emitter-to-extractor separation. When the two dies are assembled, each emitter tip sits centered underneath a grid aperture.

The extractor grid and emitter dies are fabricated using contact lithography starting with 1 mm thick, double-side polished, n-doped, 6"-diameter silicon wafers with a resistivity of 0.01-0.02 $\Omega \cdot$cm. The process flow to fabricate the extractor grid dies is shown in Figure 2A. First, a 500 nm thick thermal oxide is grown on the wafer. Next, alignment marks are etched into the wafer front side, and both sides of the wafer are coated with a 250 nm thick silicon-rich silicon nitride film. Then, the nitride and oxide films on the front side are removed using plasma and buffered oxide etching (BOE), respectively. Twenty microns of photoresist is spun onto the front side of the wafer and the features that create the aperture recess and the four springs are transferred; these features are etched to a depth

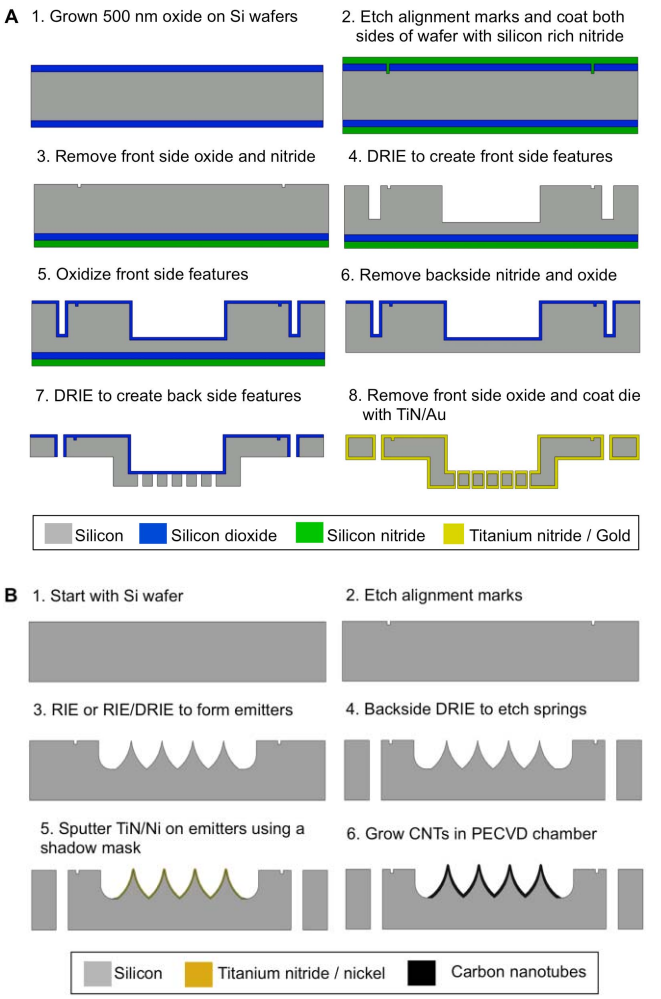

Fig. 2. (A) Process flow to fabricate the extractor grid dies; (B) process flow to fabricate the emitter dies.

of 750 μm using deep reactive-ion etching (DRIE), and the photoresist is removed. Next, a 1.5 μm-thick thermal oxide is grown on the wafer, and the backside nitride and oxide layers are removed using plasma. Twenty microns of photoresist is spun onto the backside of the wafer and the features that define the array of apertures and a recess around the edge of the die are transferred. The front side of the wafer is mounted onto a quartz wafer. Subsequently, a backside DRIE step through-etches the apertures and creates a 600 μm-deep recess around the edge of the die. The silicon wafer is released from the quartz wafer, the front side oxide is removed using diluted HF, and the dies are detached from the wafer by manually breaking thin tethers. Finally, a thin titanium nitride (10 nm) and gold (100 nm) film stack is sputtered onto the extractor grid dies.

The process flow to fabricate the emitter dies is shown in Figure 2B. First, alignment marks are etched into the wafer front side. Next, 20 μm of photoresist is spun onto both sides of the wafer and arrays of three-notched dots are patterned in the front side photoresist to act as an etch mask to etch the emitter arrays; the notched dots are 292 μm in diameter for the arrays of 4, 9, 25, 49 and 81 emitters in 1 cm^2, and 89 μm in diameter for the arrays of 1900 emitters. In the case of the

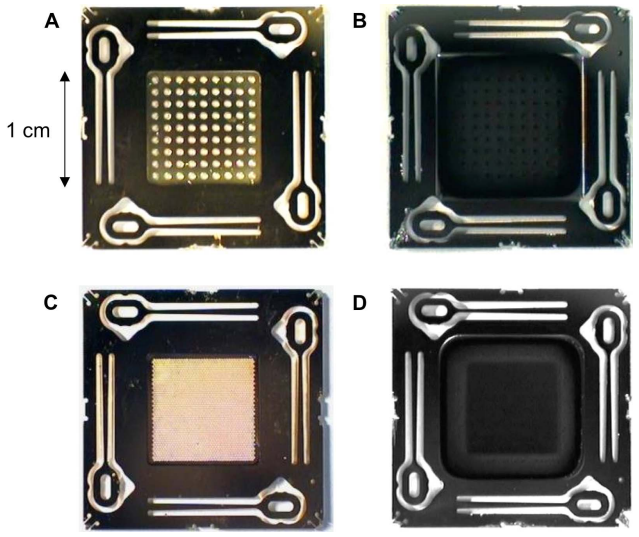

Fig. 3. (A) Extractor grid die and (B) emitter die for an array of 81 emitters in 1 cm^2; (C) extractor grid die and (D) emitter die for an array of 1900 emitters in 1 cm^2.

arrays of larger notched dots, the emitters are etched using an isotropic SF_6 reactive-ion etch (RIE) recipe; this isotropic etch produces highly sharpened silicon emitters with very smooth surface and average tip radii of 100 nm. In the case of the arrays of smaller notched dots, the emitters are etched using a recipe that alternates isotropic SF_6 steps and DRIE steps [30], [31]; this etch roughens the sidewalls of the silicon and produces silicon emitters with average tip radii of 4 μm. The front side of the wafer is mounted onto a quartz wafer and a backside DRIE step through-etches the springs. The wafer is released from the quartz wafer and the emitter are detached from the wafer by manually breaking thin tethers. Using a shadow mask, 50 nm of titanium nitride and 20 nm of nickel are sputtered onto the active area of the emitter dies. Finally, PECVD CNTs are grown as described in [26]; the CNT forest conformally coats the entire active area including the surface of the emitters. Figure 3 shows the emitter and extractor dies of sparse and dense emitter arrays.

Emitter dies with different numbers of emitters were fabricated. A first set of dies contains arrays of 4, 9, 25, 49, and 81 emitters in 1 cm^2; these devices are collectively referred to in the text as the 'sparse' emitter arrays. Their emitters are 300 μm to 350 μm tall, have a sidewall taper angle of 55° from the horizontal, and are arranged with square packing. The corresponding extractor grid dies contain apertures that are 500 μm in diameter and 250 μm thick. A second set of emitter dies contains 1900 emitters in 1 cm^2, and these are referred to in the text as the 'dense' emitter arrays. Their emitters are 450 μm tall with a sidewall taper angle of 80° from the horizontal and have hexagonal packing. The corresponding extractor grid dies contain circular apertures that are 200 μm in diameter and 250 μm thick. For electrical characterization, the assembled emitter and extractor dies are placed into a polyether ether ketone (PEEK) fixture, and electrical contact is made to the back side of the emitter die and to the front side of the extractor grid die (Figure 4A). SEM images of the emitter

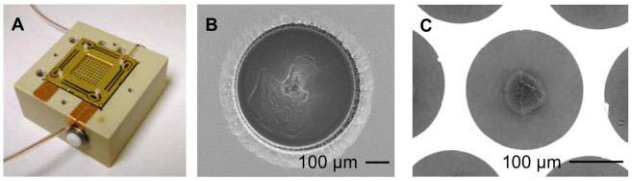

Fig. 4. (A) Assembled device in the PEEK fixture; SEM images showing the alignment of an emitter tip with an extractor aperture for (B) a sparse array and (C) a dense array.

tips sitting centered below the extractor grid apertures are shown in Figures 4B and 4C. The thickness of the polyimide spacers sets the distance G between the emitter tip and the edge of the extractor grid aperture, as shown in Figure 1D. The start-up voltage V_{start} for emission from an externally-fed electrospray emitter is [10]

$$V_{start} = \sqrt{\frac{\gamma R}{\varepsilon_o}} ln\left(\frac{2G}{R}\right) \tag{2}$$

where R is the emitter tip radius and $2G \gg R$. For low operating voltages, the distance G should be small. Ideally, the thickness of the polyimide spacers should be chosen so that G is comparable to the radius of the grid apertures.

An SEM image of an emitter that is part of a sparse emitter array is shown in Figure 5A, along with magnified images of the conformal CNT forest on the emitter surface; SEM images of CNT-coated emitters from a dense emitter array are shown in Figure 5B. The CNTs are 2 μm tall and have an average outer diameter of 100 nm. The solid volume fraction of the CNTs in the CNT film is estimated from top-view SEM images to be 12%. The CNTs are oriented vertically in the case of the sparse emitters, as is expected of PECVD CNTs because of the electric field present during growth [26], [32], and oriented more randomly in the case of the dense emitters. The difference in orientation may be due to the difference in the surface roughness of the two emitters: the sparse emitters have a visibly smoother surface than the dense emitters. Alternatively, it is possible that the CNTs are not as well aligned to the direction of the electric field present during growth in the dense emitter arrays due to the steep sidewalls of the emitters; similar results are reported in [33]. Nonetheless, both CNT films are highly wetting and the difference in orientation of the CNTs is not observed to affect their performance as a wicking medium.

III. Experimental Characterization

A. Wetting Properties of CNT Wicking Medium

Pristine CNTs are poorly wetted by water and organic solvents and hence functionalization is needed to improve their wettability [34]. However, PECVD CNT forests are highly wetting because they have a high defect density, which results in a high surface energy. Characterization of the PECVD CNT forest using Raman spectroscopy reveals that the ratio of the intensity of the D peak to the G peak is 1.1 (Figure 6), consistent with CNTs with a high density of atomic defects. The high surface energy of the CNTs combined with the nanostructured roughness of the CNT forest creates a highly wetting surface. A drop of EMI-BF_4 placed on the surface

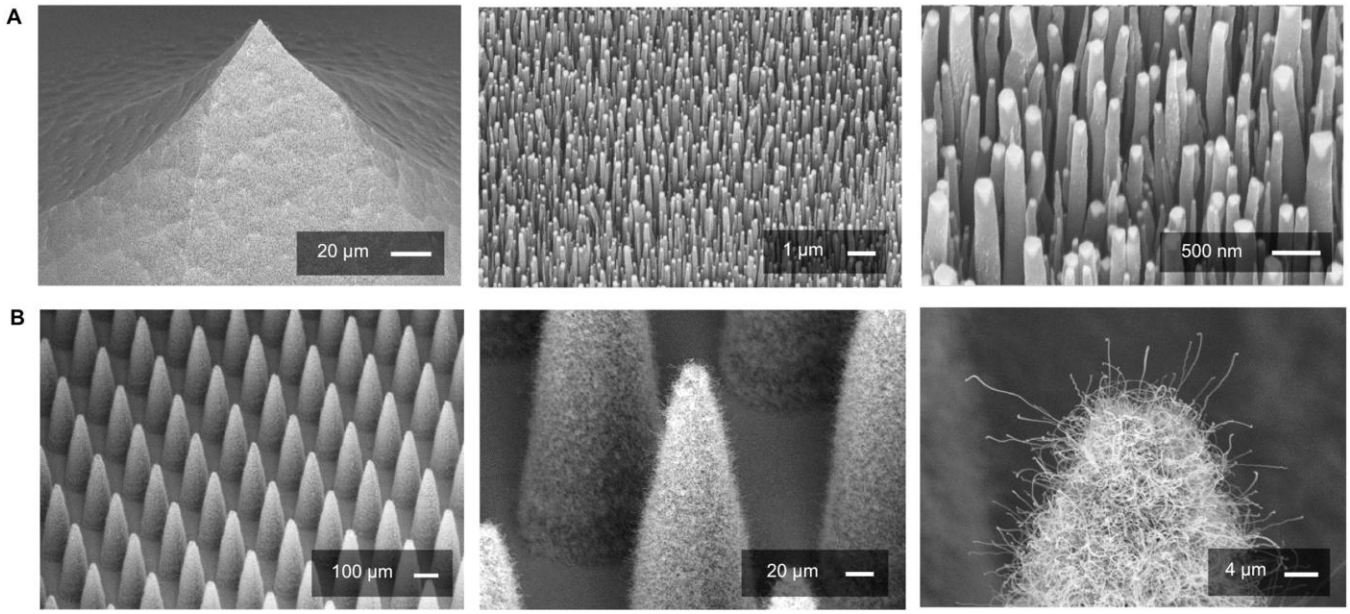

Fig. 5. (A) SEM images of an emitter that is part of a sparse emitter array, along with close-up images of the CNTs grown on the emitter surface. (B) SEM images of a dense array of emitters coated with CNTs, along with close-up images of a single emitter and emitter tip.

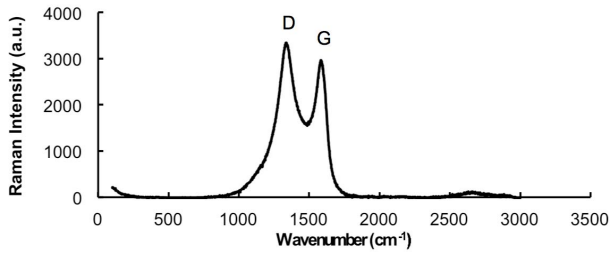

Fig. 6. Raman spectrum of the CNT forest grown on the devices.

of a CNT forest spreads spontaneously across the emitter array, impregnating the surface and coating the emitter tips, as shown in Figure 7. The liquid stops spreading once it reaches the outer edge of the CNT-coated active area because of the difference in wetting properties of the CNT film and the surrounding silicon. SEM imaging of the emitters after application of the ionic liquid reveals that a thin film of liquid coats the surface of the emitters and the excess liquid pools at the emitter bases.

The wetting properties of the CNT film are time-dependent: the CNTs are most wetting immediately after growth, and a gradual drop in the spreading rate of EMI-BF_4 over the CNT film is observed several weeks after growth. Electrospray tests are typically conducted within several days of growth of the CNT forest on the surface of the emitters, but devices tested up to one month after CNT growth show no detectable difference in performance.

B. Device Characterization Procedure

For each test, a drop of 0.5 μL (sparse arrays) or 5 μL (dense arrays) of EMI-BF_4 is deposited onto the active area of the emitter die. The liquid spreads spontaneously to coat

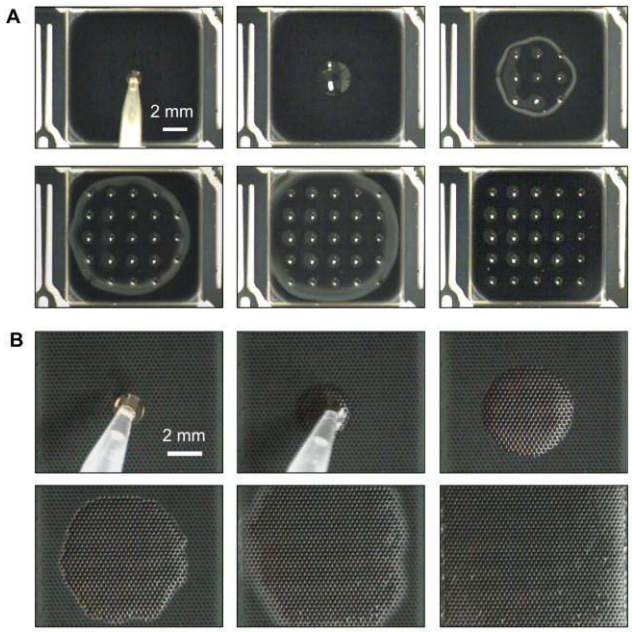

Fig. 7. Images showing (A) the spreading of 0.5 μL of EMI-BF_4 on the CNT-coated surface of an emitter die with an array of 25 emitters in 1 cm^2 and (B) the spreading of 5 μL of EMI-BF_4 on the CNT-coated surface of an emitter die with an array of 1900 emitters in 1 cm^2.

the surface of the emitters. To assemble the electrode grid, the four dowel pins are inserted into the emitter die by drawing back each spring and sliding a dowel pin into the dowel slot; releasing the spring clamps the dowel pins in place. Polyimide spacers are placed over the dowel pins. The springs on the extractor grid die are drawn back and the extractor grid die is slid into place over top of the emitter die. The assembled emitter and extractor dies are placed into

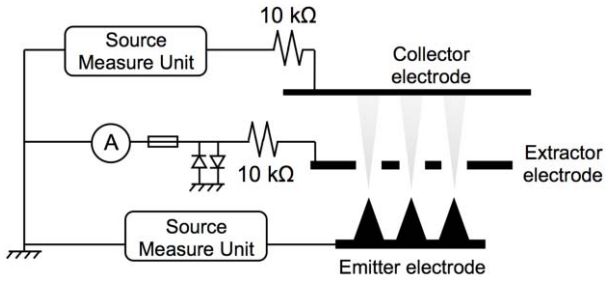

Fig. 8. Schematic of the electrospray testing electrical circuit.

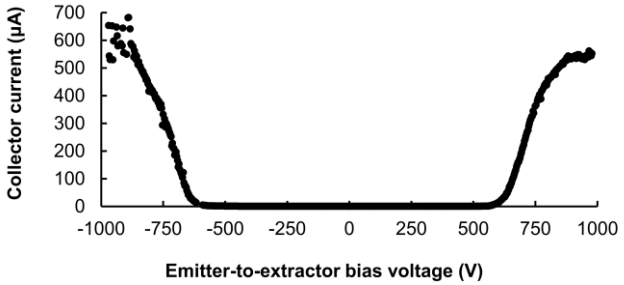

Fig. 9. Magnitude of the collector current as a function of the emitter-to-extractor bias voltage for an electrospray source with 1900 emitters in 1 cm^2.

a PEEK fixture that permits electrical contact to the back side of the emitter die and to the top side of the extractor grid die. The devices are tested in vacuum at a pressure in the 1×10^{-6} Torr range.

A triode configuration is used to conduct quasi-static electrical characterization of the electrospray sources (Figure 8). A 2 cm by 2 cm mirror-polished silicon collector electrode is placed 3.5 mm in front of the device to measure the emission current and collect imprints of the emission. A Keithley 2657A source-measure unit (SMU) is used to bias the emitter electrode up to $\pm$2000 V, applying a discretized triangular wave between the emitter and extractor electrodes with typical voltage step of 3 V to 5 V, with a wave period in the 30 s range; the alternation of the polarity of the emission due to the triangular wave helped to slow down a build-up of ions that could trigger electrochemical effects on the emitters [21]. A Keithley 6485 picoammeter measures the current intercepted by the grounded extractor grid. A Keithley 2657A SMU applies a bias voltage up to $\pm$1000 V to the collector electrode (with opposite polarity to the polarity of the emitted beam) using a square wave with a period identical to the period of the triangular wave. A pair of diodes and a fuse protect the picoammeter from current surges. A LabVIEW script is used to control the SMUs and the picoammeter and to collect the experimental data. After a series of electrospray tests are conducted on a device, the liquid begins to deplete. To replenish the liquid, the device is removed from vacuum and the two electrodes are separated by removing the dowel pins. The extractor electrode is cleaned with acetone, rinsed with water and dried with an air gun. The emitter electrode is gently rinsed in a water bath and dried under a low vacuum ($\sim$1 Torr). The collector electrode is replaced each time the liquid is replenished.

C. Current-Voltage Characteristics

Across all devices, three different phases of emission are observed: an initial over-wet phase, a steady phase, and a depletion phase. Similar behavior was displayed by our previous generation of surface-fed emitters that use black silicon as the wicking material [13]. With fresh liquid applied to the emitter surface, emission is initially noisy and unstable, punctuated by current surges. This behavior is thought to be due to emission of excessive liquid initially present at the surface of the emitter tips. Subsequently, emission steadies and is marked by stable current emission that varies as a function of the applied emitter-to-extractor bias voltage. The length of time that the emission can operate in the steady phase depends on the initial applied volume of liquid deposited, the number of emitters, and the level of the current output. Gradually, the current output at a given bias voltage is observed to decline as the liquid depletes.

Typical current-voltage characteristics in the steady phase for both sparse and dense emitter arrays are shown in Figure 9. The curves show a strong non-linear dependence between the current and the bias voltage. Four general emission regions are identified: (i) no significant emission occurs below the start-up voltage, (ii) beyond the start-up voltage the current increases first exponentially and then (iii) linearly, and finally, (iv) there is a saturation region in which the current levels off and becomes noisy, with little further increase in current with increased bias voltage. Below the start-up voltage, the electric field at the emission sites is low and no measurable emission occurs. Beyond the start-up voltage, the exponential dependence of the current on the voltage is a good indication that ion emission is occurring. For droplet emission, output currents are more or less constant for voltages around the start-up voltage at a fixed flow rate [18]. In contrast, ion emission is barrier limited and therefore small changes in the voltage produce large changes in the current, which is the behavior observed. At higher voltages, the transition to a linear dependence between the current and the applied voltage suggests that the flow becomes ballasted. As the emitter current increases, the large hydraulic impedance of the CNT forest limits the supply of liquid to the emission site, and emission becomes supply limited. The current continues to increase linearly until a maximum current is reached. At the saturation current, the current ceases to increase, the fraction of intercepted current at the extractor grid electrode rises, and the current at the collector electrode becomes noisy. Such behavior may be the result of multiple Taylor cones forming that may lead to increased intercepted current.

Typical current-voltage characteristics showing the maximum measured emission current from both the sparse and dense emitters are shown in Figure 10; the current is plotted up to the saturation current for clarity. For the sparse emitters, symmetric emission is observed in both polarities with as much as 5 μA per emitter tip, more than five times higher than the best values previously reported in the literature for a plurality of electrospray emitters operating in parallel [6],

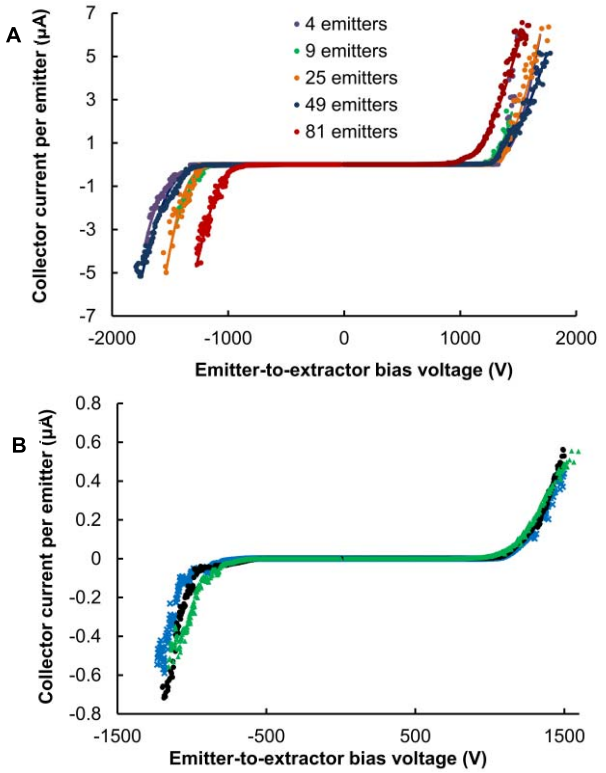

Fig. 10. Collector current per emitter as a function of emitter-to-extractor bias voltage for (A) the electrospray sources with 4, 9, 25, 49 and 81 emitters in 1 cm^2 and (B) the electrospray sources with 1900 emitter in 1 cm^2 showing the results of three different series of voltage sweeps.

[13], [16]. The operating voltages are lower for the array of 81 emitters than for the sparse emitter arrays, likely because the emitters in the array of 81 emitters are on average 50 μm taller than the emitters in the smaller arrays. Defining the start-up voltage as the voltage at which the collector current per emitter reaches 5 pA, start-up voltages as low as 470 V are observed for the array of 81 emitters, and 520 V for the smaller sparse emitter arrays. While there is some shift in the operating voltages due to differences in emitter height and emitter-to-extractor aperture separation across the different devices, the similar curve shapes and slopes of the per-emitter current-voltage curves for the different sparse emitter array sizes demonstrate that all of the emitters operate uniformly. For the sparse emitter arrays, the current per emitter increases exponentially up to a value of about 300 nA, and then increases more or less linearly with an average slope of 15 nA/V until the saturation current is reached. For the array of 81 emitters, the maximum measured emission current is 650 μA (650 μA), corresponding to a maximum current per emitter of 8 μA. For the dense emitter arrays, start-up voltages consistently as low as 470 V are measured; the emission current increases exponentially for current below about 100 nA per emitter, and then increases more or less linearly with an average slope of 2.3 nA/V until the saturation current is reached. The maximum measured emission current from these arrays is 1.35 mA (1.35 mA), corresponding to a maximum current per emitter of 0.7 μA.

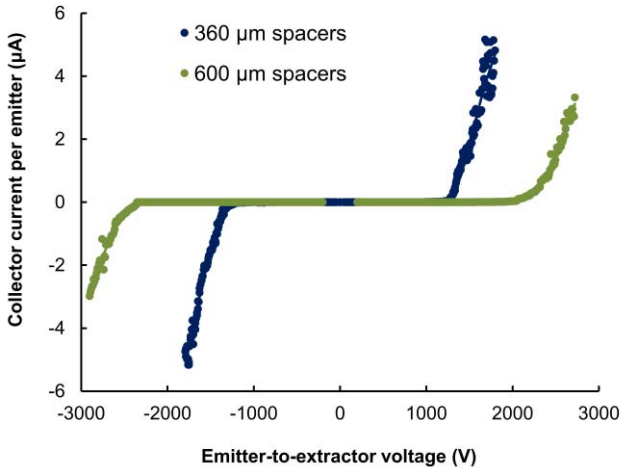

Fig. 11. Per-emitter collector current vs. emitter-to-extractor bias voltage for an array of 49 emitters with 360 μm and 600 μm spacing between the emitter and extractor grid electrodes.

For the sparse emitter arrays, the devices typically have ~80% transmission in both polarities; for the dense emitter arrays, the transmitted current can be as high as 60% in both polarities. The difference in aperture sizes between the dense and sparse emitter arrays is expected to account for the higher intercepted current for the dense emitter arrays. For both the sparse and dense emitter arrays the intercepted current is higher than previously reported for black silicon-coated devices [13], and could be reduced by increasing the diameter of the extractor grid apertures, though at the cost of increasing the operating voltage, or by reducing the thickness of the aperture grid.

Electrospray tests were conducted with different thickness spacers separating the emitter and extractor grid electrodes. For both the dense and sparse emitters, the best performance was obtained using 360 μm thick spacers. Thicker spacers result in higher operating voltages. Using 240 μm thick spacers between the electrodes, liquid bridges occasionally form between the emitter tips and the extractor grid during operation, leading to a short circuit. Using 360 μm thick spacers, liquid bridges do not form between the electrodes and the lowest operating voltages are observed. The current-voltage characteristics of an array of 49 emitters during the steady emission phase are shown in Figure 11 with both 600 μm thick (G = 320 μm) and 360 μm thick (G = 250 μm) spacers between the emitter and extractor grid electrodes. The start-up voltage is 520 V for the 360 μm spacers and 1300 V for the 600 μm spacers, demonstrating that reducing the distance between electrodes substantially reduces the operating voltages.

D. Emission Modeling

The current-voltage characteristics indicate that the emitted current increases exponentially at low voltages and depends on ionization at the liquid surface due to the electric field, while at high voltages the emission current from each emitter is limited by the supply of liquid to the emission site due to the high hydraulic impedance. We propose to model the emission from

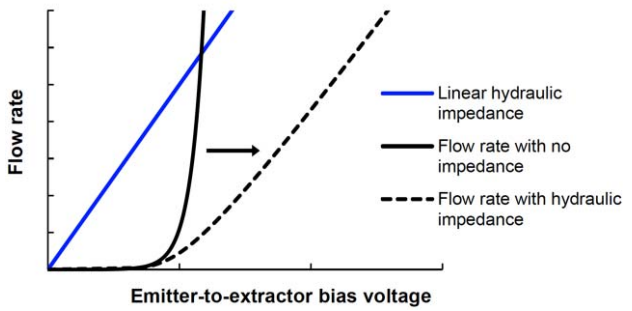

Fig. 12. Schematic plot showing the effect of placing a linear hydraulic impedance in series with an electrospray emission site on the flow rate.

our surface-fed electrospray sources by an electrical circuit with a voltage source in series with a diode and a resistor [4], [13]. The current I across a diode as a function of the bias voltage V_d is

$$I = C_1(e^{C_2 V_d} - 1) \tag{3}$$

where C_1 and C_2 are constants; the voltage drop V_r across a linear resistor with resistance R is $V_r = IR$. The applied voltage V can therefore be related to the emitted current I from the electrospray source according to

$$V = \frac{1}{C_2} ln\left(\frac{I}{C_1} + 1\right) + IR. \tag{4}$$

The constants C_1 and C_2 depend on the parameters of the experimental setup, including the emitter-to-extractor separation distance, the emitter height and tip radius, the temperature, and the physical properties of the liquid. For emission in the ionic regime, the volumetric flow rate Q can be expressed as a function of the output current I according to

$$Q = \frac{I\langle m/q\rangle}{\rho} \tag{5}$$

where $\langle m/q\rangle$ is the average mass-to-charge ratio of the emitted particles and ρ is the density of the liquid. Therefore,

$$V = \frac{1}{C_2} ln\left(\frac{Q\rho}{C_1\langle m/q\rangle} + 1\right) + \frac{Q\rho R}{\langle m/q\rangle}. \tag{6}$$

The effect of the hydraulic impedance in series with the ion emission site is shown schematically in Figure 12. Without any hydraulic impedance, the output flow rate increases exponentially with the applied bias voltage; this flow is barrier-limited. With a linear hydraulic impedance in series with the emission site, the flow increases exponentially at low bias voltages (barrier-limited flow), and linearly at high bias voltages due to the ballasting effect (supply-limited flow). The value of the resistance R is expected to depend on the viscosity of the liquid and the permeability of the porous medium. Employing the analysis outlined in [35], the permeability of the forest is estimated at $K = 3.3 \times 10^{-15}$ m^2, considering a staggered arrangement of pillars with mean pillar diameter of 100 nm and a solid volume fraction of 12%. This model shows an excellent fit to the current-voltage data for both the sparse and dense emitter arrays, with average calculated values for R of 30 MΩ (sparse emitters) and 330 MΩ (dense emitters).

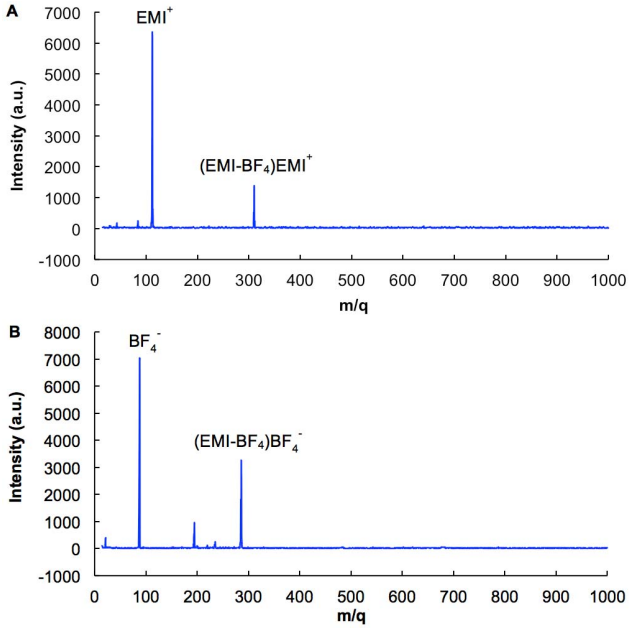

Fig. 13. Mass spectrum of the electrospray emission for an array emitting (A) positive ions and (B) negative ions.

E. Mass Spectrometry Characterization

Mass spectrometry of the electrospray is conducted at a pressure in the range of 1×10^{-7} Torr using a commercial quadrupole mass spectrometer (Ardara Technologies, Ardara PA) capable of measuring between 15 u and 10000 u with up to 10000:1 resolution assuming the species that compose the sample are singly ionized. Spectra of the emission from a dense electrospray source in both the positive and negative polarities are shown in Figure 13. In the positive polarity, the two main peaks observed in the mass spectrometry data correspond closely to the masses of the monomer EMI^+ (111.2 u) and the dimer $(EMI\text{-}BF_4)EMI^+$ (309.2 u); no peaks for the trimer or larger ions are observed. In the negative polarity, peaks corresponding to the monomer BF_4^- (86.8 u) and the dimer $(EMI\text{-}BF_4)BF_4^-$ (284.8 u) are observed, along with minor but distinguishable peaks corresponding to the trimer $(EMI\text{-}BF_4)_2BF_4^-$ (482.8 u) and the tetramer $(EMI\text{-}BF_4)_3BF_4^-$ (680.8 u). These results demonstrate that the electrospray source operates in the ionic regime, with emission consisting mainly of monomers and dimers. On average, the output ion beam contains 85% monomers and 15% dimers for positive ions, and 72% monomers and 28% dimers for negative ions. In both cases, the average mass per unit charge $\langle m/q\rangle$ is 1.5×10^{-6} kg/C. The mass spectra obtained in this work are in agreement with those reported in the literature [13], although the data in this work have visibly higher resolution. Similar mass spectra were obtained using the sparse emitter arrays. We did not see any other peaks, in particular a broad peak centered around 6258 u that other researchers have reported for some electrospray emitters that use $EMI\text{-}BF_4$ [36]; this peak is associated with droplet emission.

F. Collector Imprints

Imprints on the collector electrode are analyzed to study the deposition patterns and the array emission uniformity. Typical

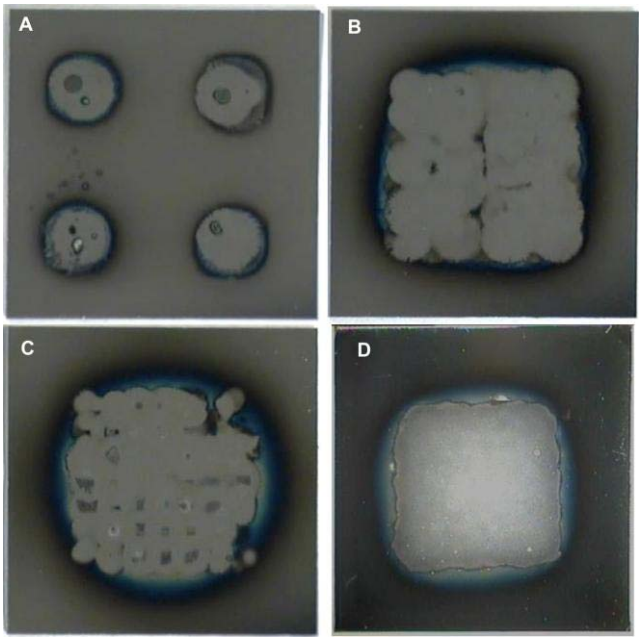

Fig. 14. Electrospray imprints on the collector electrode for an array of (A) 4 emitters, (B) 25 emitters, (C) 49 emitters, and (D) 1900 emitters. Each collector electrode is a 2 cm by 2 cm polished silicon plate.

collector imprints are shown in Figure 14. The pattern of the imprints on the collector plates matches the emitter layouts, indicating that all of the emitters turn on. Additionally, the intensity of the imprints is uniform across the plate, so the emitters all emit in a uniform manner. For the arrays of 4 and 9 emitters, circular imprints are left on the collector plates; each imprint contains an inner circle of what appears to be polished silicon with little additional coating, and a dark ring at the periphery. Based on the imprints of the array of 4 emitters, a beam divergence semi-angle of 38° is estimated. Energy-dispersive X-ray spectroscopy (EDX) analysis shows barely detectable traces of carbon and fluorine within the inner circle, and stronger carbon and fluorine traces in the dark outer ring. As has been suggested previously [13], it is thought that material deposited in the area immediately above an emitter tip is sputtered away, leaving an inner circular region with little deposited material. The deposits are darkest a short radial distance from the emission site where less sputtering occurs, and from there the deposits gradually fade further away from the emission site. For larger array sizes, the diameter of the lightly-coated inner circles decreases, probably caused by pinching of the individual beams due to charge repulsion. For the arrays of 81 and 1900 emitters, imprints corresponding to individual emitter tips are difficult to identify, leaving a 1 cm by 1 cm square region in the center of the collector plate that EDX analysis indicates to be silicon with little additional coating. In the case of the arrays of 1900 emitters, the silicon within this square region is discolored and the originally polished surface appears roughened. For the larger emitter array sizes (25, 49, 81, and 1900 emitters), the darkest deposits are located in a ring surrounding the periphery of the center 1 cm by 1 cm square region, and the deposits

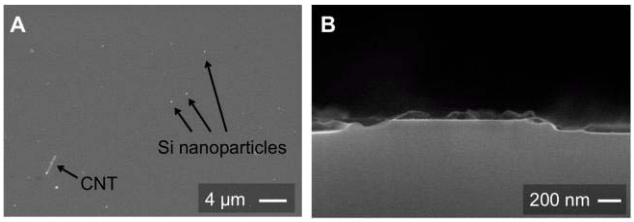

Fig. 15. (A) SEM image of the deposits on the collector plate from the emission from an electrospray source, showing occasional CNTs and silicon nanoparticles on the collector plate. (B) Edge-view of the cross-section of a collector plate showing evidence of etching of the silicon.

gradually fade towards the edge of the collector plate; this area corresponds exactly to the active area of the electrospray source. The intensity of the carbon and fluorine peaks in the EDX spectra is highest in the outer ring and weakest within in the inner 1 cm by 1 cm area.

SEM images of the collector plates reveal that a small number of CNTs can be found deposited onto the collector plate within the 1 cm by 1 cm center region, as shown in Figure 15A; a larger number of CNTs are deposited onto the collector plates in the case of the dense emitter arrays. Small, round nanoparticles with diameters on the order of 400 nm and smaller are also observed on the collector plates. These nanoparticles are identified as silicon using EDX analysis, and are found in the 1 cm by 1 cm center on the collector plate and not in the surrounding area, indicating that they are a result of the electrospray process. No traces of nickel or titanium are measured on the collector plates.

To examine the collector plates for etching, collector plates are cleaved and the cross-sections of the plates are examined in an SEM. Clear signs of etching are seen on the collector plates from emission from the dense emitters, with as much as 110 nm of etched silicon (Figure 15B).

The CNTs were intended to stay adhered to the emitter surface, and the presence of CNTs on the collector plates is an unintended result. The CNTs must be pulled from the surface of the emitter electrode by the electric field, indicating that the base of a subset of the CNTs is not sufficiently well anchored to the surface of the emitters. The higher number of CNTs on the collector plates from the dense emitters may be an indication that adhesion is better in the case of the sparse emitters. Adhesion of CNTs to a substrate is correlated to the strength of the electric field during growth. Since the CNTs grown on the emitters in the sparse emitter arrays are much better aligned to the direction of the electric field than the CNTs grown on the dense emitters, it is postulated that the CNTs on the emitters in the dense arrays may have weaker adhesion to the underlying substrate. Nonetheless, the number of CNTs deposited on the collector plates is very small compared to the number of CNTs in the forests, so little overall degradation of the forest occurs. The CNT detachment seems not to be related to the magnitude of the flow rate per emitter because the emitters from the sparse emitter arrays can deliver up to an order of magnitude more flow rate than the emitters from the dense arrays. The mass spectrometry results show emission of monomers and dimers, so if CNTs

are emitted below these current levels then the CNTs must be emitted without accompanying droplets. It is plausible that CNT emission occurs only during the noisy, saturation period that is observed at the highest applied bias voltages, and that below the saturation current emission is ionic; the emission of CNTs could also take place during the over-wetting phase. Further investigation is merited to identify the exact conditions of the deposition of the CNTs onto the collector plates.

The origin of the silicon nanoparticles on the collector plates is also unknown. Their presence on the collector plates must be a result of the electrospray emission process because the nanoparticles are highly localized to the region on the collector electrode directly above the emitter array. These nanoparticles might possibly be the result of the etching of the silicon collector plate, or be a product of a chemical reaction between the silicon and the ionic liquid.

G. Thrust and Specific Impulse Estimates

The thrust from an electrospray source can be estimated based on the measured emission current and the mass spectrometry of the beam. An expression for thrust T is [7]

$$T = \sqrt{2\dot{m}\eta_o P_{in}} \tag{7}$$

where $\dot{m}$ is the total mass flow rate exiting the electrospray source, η_o is the overall thrust efficiency, and P_{in} is the electric power supplied to the thruster, i.e., the applied voltage V times the total output current I. The mass flow rate can also be expressed in terms of the output current as

$$\dot{m} = I\left\langle m/q \right\rangle. \tag{8}$$

The overall thrust efficiency is given by [37]

$$\eta_o = \eta_i \cdot \eta_{tr}^2 \cdot \eta_\theta \cdot \eta_E \cdot \eta_p \tag{9}$$

where η_i is the ionization efficiency, η_{tr} is the transmission efficiency, η_θ is the angular efficiency, η_E is the energy efficiency and η_p is the polydispersive efficiency. Both the ionization efficiency and the energy efficiency are taken to be close to 1 for the case of electrospray of EMI-BF_4 in the ionic regime [4]. Using the analysis outlined in [37], the angular efficiency is calculated to be 91.5% for an upper-bound beam divergence semi-angle of 38°. The polydispersive efficiency is calculated to be 91.9% for negative ions and 95.5% for positive ions. The expression for thrust in equation (7) can be rewritten in terms of the measured collector current as

$$T = I_{coll}\sqrt{2\,V\left\langle m/q \right\rangle \eta_i\,\eta_\theta \eta_E \eta_p} \tag{10}$$

where I_{coll} is the current that reaches the collector electrode. The specific impulse I_{sp} is given

$$I_{sp} = \frac{T}{\dot{m} g} \tag{11}$$

where g is the gravitational constant. Calculated thrust as a function of the emitter-to-extractor bias voltage is plotted in Figure 16 for both sparse and dense emitter arrays assuming ionic emission in all cases up to the maximum current.

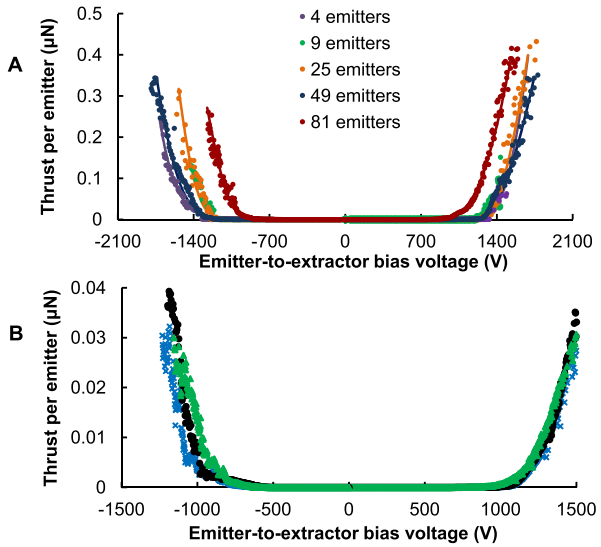

Fig. 16. Calculated thrust per emitter for the (A) sparse and (B) dense emitter arrays.

TABLE I
MAXIMUM ESTIMATED THRUST AND SPECIFIC IMPULSE

Array size	Maximum thrust	Maximum thrust per emitter	Specific impulse at max current
4	0.9 μN	0.23 μN	4235 s
9	1.2 μN	0.13 μN	4463 s
25	10.8 μN	0.43 μN	4615 s
49	17.1 μN	0.34 μN	4595 s
81	33.6 μN	0.41 μN	4297 s
1900	75 μN	0.039 μN	3691 s

The maximum calculated values of thrust and specific impulse are listed in Table 1. The highest calculated thrust is 75 μN for the array of 1900 emitters, and the largest thrust per emitter is 0.43 μN for the array of 25 emitter tips. Higher thrust and specific impulse by as much as a factor of two could be obtained for the array of 1900 emitters by reducing the intercepted current at the extractor grid electrode. The thrust per emitter in the sparse emitter arrays is about an order of magnitude larger than in the dense emitter arrays; it seems possible that an array of about 200 emitters in 1 cm^2 could outperform the array of 1900 emitters in 1 cm^2, suggesting perhaps an optimal limit in the miniaturization and emitter area packing using the current device architecture.

IV. DISCUSSION

For EMI-BF_4, the minimum flow rate Q_{min} below which emission is expected to be ionic is 3.5×10^{-15} m^3/s, considering a surface tension of 0.054 N/m, a relative electrical permittivity of 12.8, a mass density of 1285.3 kg/m^3 and an electrical conductivity of 1.36 S/m [38], [39]. At the maximum measured currents, emission of 0.7 μA per emitter for the dense emitters corresponds to a flow rate per emitter of 8.2×10^{-16} m^3/s, and 5 μA per emitter for the array of 81 emitters corresponds to a flow rate per emitter of

5.8×10^{-15} m^3/s, using equation (5) and assuming ionic emission up to the maximum emission current. In both case, the flow rates fall close to the value of Q_{min}.

In its current design, the electrospray source serves as a model to study emission from surface-fed emitters with porous coatings, and is not yet intended for long-term operation. Without a continual liquid feed, the electrospray source can only be run for relatively short periods of time before the liquid is depleted. With an initial application of 5 μL of ionic liquid, the array of 1900 emitters could operate continually at the maximum current of 0.5 μA per emitter for 53 minutes, while the array of 81 emitters could operate at an output current of 5 μA per emitter for 18 minutes with an initial application of 0.5 μL of ionic liquid.

The CNT forest on the surface of the emitters serves as a highly effective porous medium to transport the ionic liquid to the emission sites on the surface-fed emitters, resulting in stable, uniform electrospray emission; however, it is clear from the results that good adhesion is needed between the porous medium and the emitter surface. Deposition of a pore-free, conformal thin film coating over the CNT forest to improve adhesion to the underlying surface is an option to explore. Platinum would be a good candidate as a coating material because it can be conformally sputtered and has been shown to be highly resistant to the electrochemical effects from electrospraying EMI-BF_4. Nanostructured surface coatings on the silicon emitters are not limited to CNT forests; for example, a forest of zinc oxide nanowires could be grown conformally on non-planar structures such as the silicon emitters with a great deal of control over the morphology of the nanowire forest by tuning the growth conditions [40].

Cross-sections of the collector plates show that the silicon has been etched by as much as 110 nm; the silicon is likely to be etched through sputtering, due to collisions of highly energetic ions with the silicon surface. Etching using these sources is therefore a technology with great promise as a nanomanufacturing technique on par with etching using liquid metal ion sources, with the additional advantage of providing multiplexed high-throughput etching over broad areas.

V. Conclusion

The first demonstration of a MEMS multiplexed electrospray source with an integrated extractor grid and CNT flow control structures for low-voltage high-throughput electrospray ion emission from ionic liquids in vacuum has been reported. Using electrospray sources with 4, 9, 25, 49, 81 and 1900 emitters in 1 cm^2, symmetric emission in both polarities with as much as 5 μA per emitter tip is obtained, with start-up voltages as low as 470 V and transmission as high as 80% through the extractor grid. Maximum emission currents of 1.35 mA (1.35 mA/cm^2) have been measured using arrays of 1900 emitters in 1 cm^2. Imprints on the collector electrodes and uniform slopes in the current-voltage curves for different emitter array sizes demonstrate that emission is uniform across the emitter arrays and that flow to the emitters is ballasted. Mass spectrometry characterization confirms that emission occurs in the ionic regime, and etching of the collector plate is observed. Future work should address adhesion of the CNT film to the emitter surface, long-term operation of the electrospray source and focus on improving extractor grid transmission for the dense arrays of emitters.

References

[1] G. I. Taylor, "Disintegration of water drops in an electric field," *Proc. Roy. Soc. London A*, vol. 280, no. 1382, pp. 383–397, 1964.

[2] W. Deng, J. F. Klemic, X. Li, M. A. Reed, and A. Gomez, "Increase of electrospray throughput using multiplexed microfabricated sources for the scalable generation of monodisperse droplets," *J. Aerosol Sci.*, vol. 37, no. 6, pp. 696–714, 2006.

[3] I. Romero-Sanz, R. Bocanegra, J. Fernandez de la Mora, and M. Gamero-Castaño, "Source of heavy molecular ions based on Taylor cones of ionic liquids operating in the pure ion evaporation regime," *J. Appl. Phys.*, vol. 94, no. 5, pp. 3599–3605, 2003.

[4] L. F. Velásquez-García, A. I. Akinwande, and M. Martinez-Sanchez, "A planar array of micro-fabricated electrospray emitters for thruster applications," *J. Microelectromech. Syst.*, vol. 15, no. 5, pp. 1272–1280, 2006.

[5] R. Krpoun, K. L. Smith, J. P. W. Stark, and H. R. Shea, "Tailoring the hydraulic impedance of out-of-plane micromachined electrospray sources with integrated electrodes," *Appl. Phys. Lett.*, vol. 94, no. 16, pp. 163502-1–163502-3, 2009.

[6] R. S. Legge and P. C. Lozano, "Electrospray propulsion based on emitters microfabricated in porous metals," *J. Propuls. Power*, vol. 27, no. 2, pp. 485–495, 2011.

[7] B. Gassend, L. F. Velásquez-García, A. I. Akinwande, and M. Martinez-Sanchez, "A fully microfabricated externally wetted electrospray thruster," in *Proc. 43rd AIAA/ASME/SAE/ASEE Joint Propuls. Conf. Exhibit*, Cincinnati, OH, USA, Jul. 2007, no. AIAA 2007-5182, p. 8.

[8] J. Mueller, R. Hofer, and J. Ziemer, "Survey of propulsion technologies applicable to cubesats," in *Proc. JANNAF Propuls. Meet.*, Colorado Springs, CO, USA, May 2010.

[9] D. G. Courtney, H. Q. Li, and P. Lozano, "Emission measurements from planar arrays of porous ionic liquid ion sources," *J. Phys. Appl. Phys.*, vol. 45, no. 48, p. 485203, 2012.

[10] P. D. Prewett and G. L. R. Mair, *Focused Ion Beams From Liquid Metal Ion Sources*. Hoboken, NJ, USA: Wiley, 1991.

[11] A. Jaworek, "Electrospray droplet sources for thin film deposition," *J. Mater. Sci.*, vol. 42, no. 1, pp. 266–297, 2006.

[12] W. Deng, C. M. Waits, and A. Gomez, "Digital electrospray for controlled deposition," *Rev. Sci. Instrum.*, vol. 81, no. 3, pp. 035114-1–035114-6, 2010.

[13] B. Gassend, L. F. Velásquez-García, A. I. Akinwande, and M. Martinez-Sanchez, "A microfabricated planar electrospray array ionic liquid ion source with integrated extractor," *J. Microelectromech. Syst.*, vol. 18, no. 3, pp. 679–694, 2009.

[14] L. F. Velásquez-García, A. I. Akinwande, and M. Martinez-Sanchez, "A micro-fabricated linear array of electrospray emitters for thruster applications," *J. Microelectromech. Syst.*, vol. 15, no. 5, pp. 1260–1271, 2006.

[15] R. Krpoun and H. Shea, "A method to determine the onset voltage of single and arrays of electrospray emitters," *J. Appl. Phys.*, vol. 104, no. 6, pp. 064511-1–064511-8, 2008.

[16] H. Q. Li, D. G. Courtney, P. D. G. Maqueo, and P. Lozano, "Fabrication and testing of an ionic electrospray propulsion system with a porous metal tip array," in *Proc. 16th IEEE Int. Conf. Solid-State Sens., Actuators, Microsyst. Conf.*, Beijing, China, Jun. 2011, pp. 1998–2001.

[17] Y.-X. Wang, J. W. Cooper, C. S. Lee, and D. L. DeVoe, "Efficient electrospray ionization from polymer microchannels using integrated hydrophobic membranes," *Lab Chip*, vol. 4, no. 4, pp. 363–367, 2004.

[18] J. F. De La Mora and I. G. Loscertales, "The current emitted by highly conducting Taylor cones," *J. Fluid Mech.*, vol. 260, pp. 155–184, Feb. 1994.

[19] D. Garoz *et al.*, "Taylor cones of ionic liquids from capillary tubes as sources of pure ions: The role of surface tension and electrical conductivity," *J. Appl. Phys.*, vol. 102, no. 6, pp. 064913-1–064913-10, 2007.

[20] I. Guerrero, R. Bocanegra, F. J. Higuera, and J. Fernandez de la Mora, "Ion evaporation from Taylor cones of propylene carbonate mixed with ionic liquids," *J. Fluid Mech.*, vol. 591, pp. 437–459, Nov. 2007.
[21] P. Lozano, and M. Martínez-Sánchez, "Ionic liquid ion sources: Characterization of externally wetted emitters," *J. Colloid Interf. Sci.*, vol. 282, no. 2, pp. 415–421, 2005.
[22] R. Krpoun and H. R. Shea, "Integrated out-of-plane nanoelectrospray thruster arrays for spacecraft propulsion," *J. Micromech. Microeng.*, vol. 19, no. 4, p. 045019, 2009.
[23] S. Castro, C. Larriba, J. Fernandez de la Mora, P. Lozano, Y. Yoshida, and G. Saito, "Effect of liquid properties on electrosprays from externally wetted ionic liquid ion sources," *J. Appl. Phys.*, vol. 102, no. 9, pp. 094310-1–094310-5, 2007.
[24] H. Jansen, "The black silicon method: A universal method for determining the parameter setting of a fluorine-based reactive ion etcher in deep silicon trench etching with profile control," *J. Micromech. Microeng.*, vol. 5, no. 2, pp. 115–120, Jun. 1995.
[25] M. Meyyappan, L. Delzeit, A. Cassell, and D. Hash, "Carbon nanotube growth by PECVD: A review," *Plasma Sour. Sci. Technol.*, vol. 12, no. 2, pp. 205–216, 2003.
[26] M. Chhowalla *et al.*, "Growth process conditions of vertically aligned carbon nanotubes using plasma enhanced chemical vapor deposition," *J. Appl. Phys.*, vol. 90, no. 10, pp. 5308–5317, 2001.
[27] F. A. Hill, P. J. Ponce de Leon, and L. F. Velásquez-García, "High-throughput ionic liquid electrospray sources based on dense monolithic arrays of emitters with integrated extractor grid and carbon nanotube flow control structures," in *Proc. 17th IEEE Int. Conf. Solid-State Sens., Actuators, Microsyst.*, Barcelona, Spain, Jun. 2013, pp. 2644–2647.
[28] L. F. Velásquez-García, A. I. Akinwande, and M. Martinez-Sanchez, "Precision hand assembly of MEMS subsystems using DRIE-patterned deflection spring structures: An example of an out-of-plane substrate assembly," *J. Microelectromech. Syst.*, vol. 16, no. 3, pp. 598–612, 2007.
[29] B. Gassend, L. F. Velásquez-García, and A. I. Akinwande, "Precision in-plane hand assembly of bulk-microfabricated components for high-voltage MEMS arrays applications," *J. Microelectromech. Syst.*, vol. 8, no. 2, pp. 332–346, 2009.
[30] N. Roxhed, P. Griss, and G. Stemme, "Tapered deep reactive ion etching: Method and characterization," in *Proc. 14th IEEE Int. Conf. Solid-State Sens., Actuators, Microsyst.*, Lyon, France, Jun. 2007, pp. 493–496.
[31] B. Gassend, L. F. Velásquez-García, and A. I. Akinwande, "Design and fabrication of DRIE-patterned complex needle-like structures," *J. Microelectromech. Syst.*, vol. 19, no. 3, pp. 589–598, 2010.
[32] K. B. K. Teo *et al.*, "Uniform patterned growth of carbon nanotubes without surface carbon," *Appl. Phys. Lett.*, vol. 79, no. 10, pp. 1534–1536, 2001.
[33] F. A. Hill, P. J. Ponce de Leon, and L. F. Velásquez-García, "Wetting properties of carbon nanotube forests grown using plasma enhanced chemical vapor deposition on planar and non-planar substrates," in preparation.
[34] S. Hussain, R. Amade, E. Jover, and E. Bertran, "Functionalization of carbon nanotubes by water plasma," *Nanotechnology*, vol. 23, no. 38, p. 385604, 2012.
[35] A. Tamayol and M. Bahrami, "Transverse permeability of fibrous porous media," *Phys. Rev.*, vol. 83, no. 4, pp. 046314-1–046314-8, 2011.
[36] K. J. Terhune and L. B. King, "Ion and droplet mass measurements of an electrospray emitter using ExB filter," in *Proc. 32nd Int. Electr. Propuls. Conf.*, Wiesbaden, Germany, 2011, no. IEPC-2011-299, pp. 11–15.
[37] P. Lozano and M. Martinez-Sanchez, "Efficiency estimation of EMI-BF4 ionic liquid electrospray thrusters," in *Proc. 41st AIAA/ASME/SAE/ASEE Joint Propuls. Conf. Exhibit*, Tucson, AZ, USA, Jul. 2005, no. AIAA 2005-4388, p. 8.
[38] W. Martino, J. Fernandez de la Mora, Y. Yoshida, G. Saito, and J. Wilkes, "Surface tension measurements of highly conducting ionic liquids," *Green Chem.*, vol. 8, no. 4, pp. 390–397, 2006.
[39] C. Wakai, A. Oleinikova, M. Ott, and H. Weingartner, "How polar are ionic liquids? Determination of the static dielectric constant of an imidazolium-based ionic liquid by microwave dielectric spectroscopy," *J. Phys. Chem. B*, vol. 109, no. 36, pp. 17028–17030, 2005.
[40] M. Laurenti *et al.*, "Wettability control on ZnO nanowires driven by seed layer properties," *Eur. J. Inorg. Chem.*, vol. 2013, no. 14, pp. 2520–2527, 2013.

Frances Ann Hill received the Bachelor of Applied Science degree from the University of Waterloo, Waterloo, Canada in 2006, and the M.S. and PhD degrees from the Department of Mechanical Engineering, Massachusetts Institute of Technology (MIT), Cambridge, MA, in 2008 and 2011, respectively. Between 2011 and 2013, she was a Postdoctoral Associate with the Microsystems Technology Laboratories at MIT. She is currently a Research Scientist at KLA-Tencor, Milpitas, CA.

Eric Vincent Heubel received a B.S. degree from the Department of Mechanical Engineering, Michigan Technological University, Houghton, MI, in 2006, and the M.S. degree from the Department of Mechanical Engineering, Massachusetts Institute of Technology (MIT), Cambridge, MA, in 2008. He is currently working toward the PhD degree at MIT with a focus on precision micromachined plasma sensors.

Philip Ponce de Leon received the B.S. degree in Physics from New York University, New York, NY, and the B.E. degree in Mechanical Engineering from the Stevens Institute of Technology, Hoboken, NJ, in 2011. He is currently working toward the S.M. degree at Massachusetts Institute of Technology, Cambridge, MA, with a focus on high-throughput electrospinning of nanofibers using MEMS.

Luis Fernando Velásquez-García (M'09-SM'10) is a Principal Scientist with the Microsystems Technology Laboratories, Massachusetts Institute of Technology, Cambridge. His research focuses on micro and nanoenabled multiplexed scaled-down systems for space, energy, healthcare, manufacturing, and analytical applications that exploit high-electric field phenomena, e.g., electrospray, electrospinning, electron impact ionization, field ionization, field emission, X-rays, and plasmas.